Iraqi Journal of Physics, 2024 *Vol. 22, No. 2, PP. 48-56*
https://doi.org/10.30723/ijp.v22i2.1226 *P-ISSN: 2070-4003*
E-ISSN: 2664-5548

Effect of Annealing Process on the Morphological, Optical and Electrical Properties of Cu:MnO Films Prepared by PLD Technique

Doaa T. Mohammed[1a] and Ghuson H. Mohammed [1b*]
[1]*Department of physics, College of Science, University of Baghdad, Baghdad, Iraq*
[a]*E-mail: duaathamer111@gmail.com*
[b*] *Corresponding author: ghuson.mohammed@sc.uobaghdad.edu.iq*

Abstract

In this study, Nd:YAG laser pulses with a wavelength of 1064 nm, a power of 500 mJ, a pulse width of 9 ns, and a repetition frequency of 6 Hz were used to hit a manganese oxide (MnO) target surface 300 times. Undoped and doped MnO were prepared with different concentrations of Cu (0.03, 0.05, 0.07, and 0.09%) prepared by PLD. Cu:MnO thin films were annealed at 473 K, and their morphological, optical, and electrical characteristics were studied. The results of the atomic force microscopic (AFM) investigation of morphological properties showed that Cu dopant impacted the creation of roughness and particle size in MnO2 films. The optical transmission was examined using a UV-Vis spectrophotometer. The highest optical absorption was noted at 0.09 dopant content. The dielectric constants' real (ε_r) and imaginary (ε_i) components, as well as the extinction coefficient (k), refractive index (n), and other optical constants, were studied. At an annealing temperature of (473 K), Hall effect studies demonstrate that all produced films exhibit P-type conductivity.

Article Info.

Keywords:
MnO Thin Films, Cu Nanoparticles, Optical Constants, Morphological Properties, PLD Technique.

Article history:
Received: Dec. 10, 2023
Revised: Mar. 05, 2024
Accepted: Mar. 11, 2024
Published: Jun. 01,2024

1. Introduction

Nanotechnology is a relatively young technology that has resulted in substantial advancements in several industries [1]. Semiconductors were created to meet the most recent gas sensor criteria [2]. A semiconductor gas sensor performs well regarding stability, sensitivity, and selectivity for gas detection [3]. Due to their distinct electronic and optical properties, nanomaterials have been investigated in numerous disciplines, such as chemistry, medicine, physics, materials sciences, biology, and pharmacy [4]. Nanomaterials have been investigated across several academic disciplines, encompassing chemistry, medicine, physics, materials sciences, biology, and pharmacy, owing to their distinctive electrical and optical characteristics [5-7]. Copper oxide (CuO) nanoparticles have been extensively used in many applications, such as catalysis, solar energy, electricity, batteries, gas sensors, and the degradation of organic dyes [8]. Manganese oxid (MnO) nanoparticles are one of the most researched metal oxides because of their unique properties. This oxide has a small band gap and a large optical constant [8]. MnO exhibits transitional properties and possesses numerous oxidation numbers, namely +2, +3, and +4; hence, it exists in diverse oxide structures, such as MnO, MnO_2, Mn_2O_3, and Mn_3O_4. The compound manganese oxide has garnered significant attention from researchers, leading to several research endeavours [9, 10]. Manganese oxide and manganese oxide nanoparticles have been synthesized via a variety of techniques, including spray pyrolysis [11], sol-gel [12], atomic layer deposition [13], thermal evaporation [14-16], pulsed laser deposition [17-19], RF magnetron sputtering [20, 21], metal-organic chemical vapor deposition [22], and electron beam technique followed by archiving post-treatment [23]. Nelson et al. [24] studied the impact of deposition temperature and substrate on the formation of manganese oxide thin films using ALD (Atomic Layer Deposition). The investigation

of various crystal morphologies of manganese oxide is of significant interest due to their notable characteristics, including a substantial specific surface area, a considerable proportion of surface atoms, and their non-toxic nature. Extensive research has been conducted on the physical and chemical properties of manganese oxide nanoparticles, as well as its diverse range of applications, including its use in catalytic processes [25], antibacterial [26], water treatment [27], and electrochemical capacitors [28]. Several techniques have been devised to create MnO nanoparticles, including the hydrothermal method, the template-assisted method, the wet chemical method, and the sol-gel method [29].

The purpose of this work was to study the effect of annealing process on the morphological, optical and electrical properties of Cu-doped MnO films at different concentrations of Cu prepared by PLD techniques.

2. Experimental

2.1. Preparation of Samples

MnO (99.99% purity) in the form of a powder, obtained by grounding the MnO with a mortar for five minutes, was mixed with different contents of Cu nanoparticles (0.03, 0.05, 0.07, and 0.09 wt%). Using a hydraulic piston form (SPECAC) at a pressure of 5 tons for 10 minutes, pellets of 1 cm in diameter and a thickness of 0.2 cm were prepared. Then, they were sintered in air at 673K for one hour before being chilled to room temperature.

2.2. Deposition of Thin Films

The synthesis pellets were utilized to form Cu-doped MnO thin films on glass substrates, which were cleaned for 15 minutes using an ultrasonic method and distilled water. To create the thin films, the pulsed laser deposition technique was used using a Nd:YAG laser of 1064 nm wavelength and 0.5 J energy. The settings were set up so that 300 laser pulses of 6 Hz repetition rate hit a target at a 45° angle. The deposition was carried out in a vacuum chamber $1x10^{-2}$ mbar pressure. The substrate was positioned 1.5 cm away from the MnO target. The thin film thickness was 200±5nm and was calculated using the interference method. Finally, thin films were thermally treated for one minute at 473 K.

2.3. Measurements

The surface morphological characteristics of the thin films were investigated using atomic force microscopy (AFM). UV-Vis spectrophotometer (Metretech SP-8001) was used to examine the thin films' optical properties. The instrument's wavelength range was from 190 to 1100 nm. The Hall effect measurements, using the Hall effect system (HMS-3000, supplied by the Ecopia company), were carried out to determine the type, mobility and concentration of the charge carriers.

3. Results and Discussions

3.1. Atomic Force Microscopic

The surface morphology of pure and Cu-doped MnO thin films was studied using AFM analysis to find the root mean square (RMS), mean diameter, and mean roughness, as shown in Fig. 1; the parameters values are tabulated in Table 1. Fig. 1 shows 3D AFM images of pure and Cu-doped MnO of different dopant content thin films; a granular surface with porous features and of spherical grains can be noted. Compared to the pure MnO thin films, Cu-doped MnO thin films have a distinct morphology, which was dramatically impacted by the incorporation of Cu ions into the lattice. With the increase of Cu content, the roughness increased from 27.96 to 79.46

nm, while RMS increased from 33.45 to 78.45 nm. Also, the grains appeared to agglomerate and grow as the Cu content increased; the surface was seen coated in dense, uniform grains. The increase in the particles size is a direct result of Cu's interstitial dopant role [30].

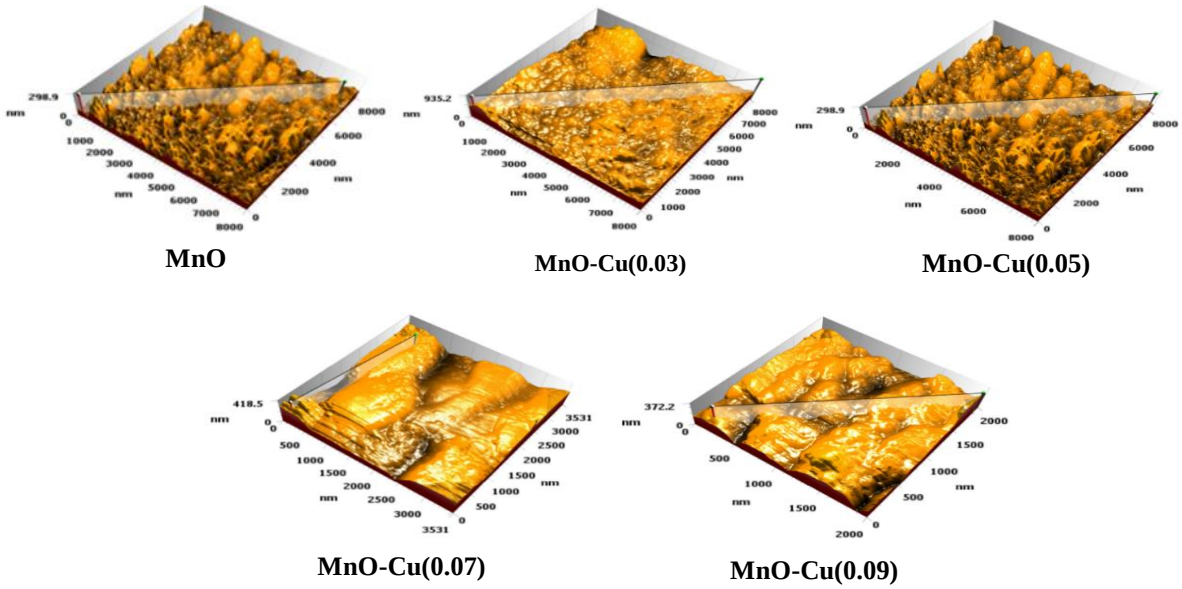

Figure 1: 3D AFM images of pure and Cu-doped MnO with different Cu content thin films.

Table 1. Average values of surface roughness, particle size and RMS for the pure and Cu-doped MnO thin films annealed at 473 K.

Sample	Avg. Diameter(nm)	Avg. Roughness(nm)	R.M.S (nm)
Pure MnO	24.57	27.96	33.45
3 % Cu:MnO	33.50	29.92	38.62
5 % Cu:MnO	61.28	45.59	60.15
7 % Cu:MnO	81.26	65.74	70.15
9 % Cu:MnO	94.91	79.46	78.45

3.2. The Optical Properties

Fig. 2 shows the absorbance spectra for pure and Cu-doped MnO films of different Cu content annealed at 473k. In general, it can be observed that the absorbance decreased with the increase of λ in the visible–near-infrared (400–1100 nm) region for all the prepared samples. Also, the absorbance increased with the increase of the Cu content. This is because of the creation of localized states in the band gap. Consequently, the samples became opaque to the incident light, hence the increase in absorbance. In a previous work [31], comparing the films prepared at room temperature to the annealed samples, it was found that heat treatment has an impact on the spectral characterization. It was observed that absorbance decreased with the increase of the annealing temperature for all prepared samples due to the films becoming more transparent.

Fig. 3 demonstrates how the extinction coefficient (k) varies with wavelength in the 400–1100 nm range for different Cu content for the thin films annealed at 473k. The k values were derived using the following relationship:

$$k = \frac{\alpha\lambda}{4\pi} \quad (1)$$

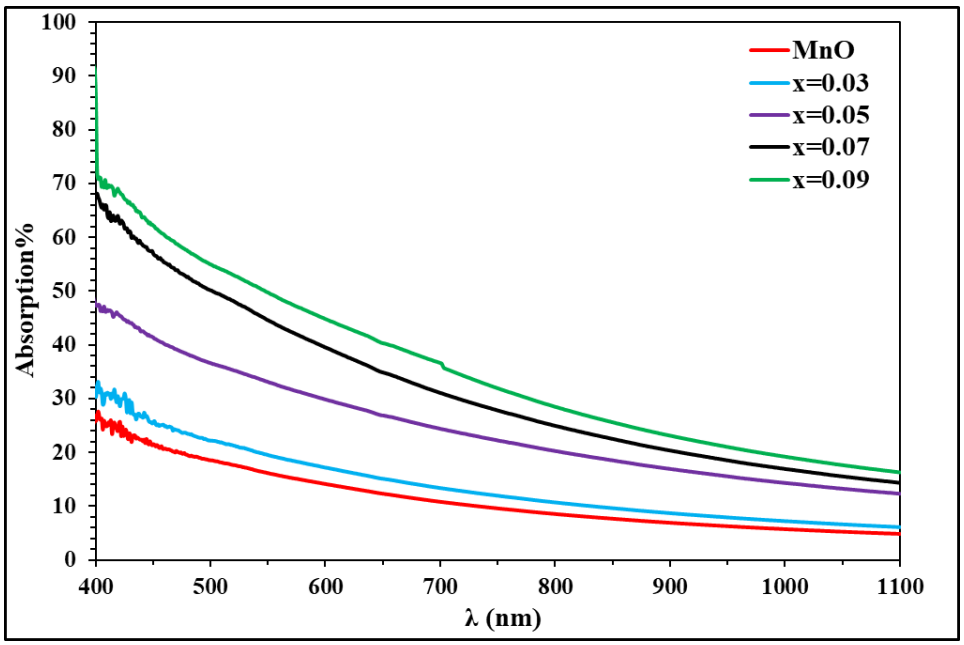

where: α is the absorption coefficient and λ is the wavelength of the incident photons. The extinction coefficient depends mainly on the absorption coefficient and, therefore,

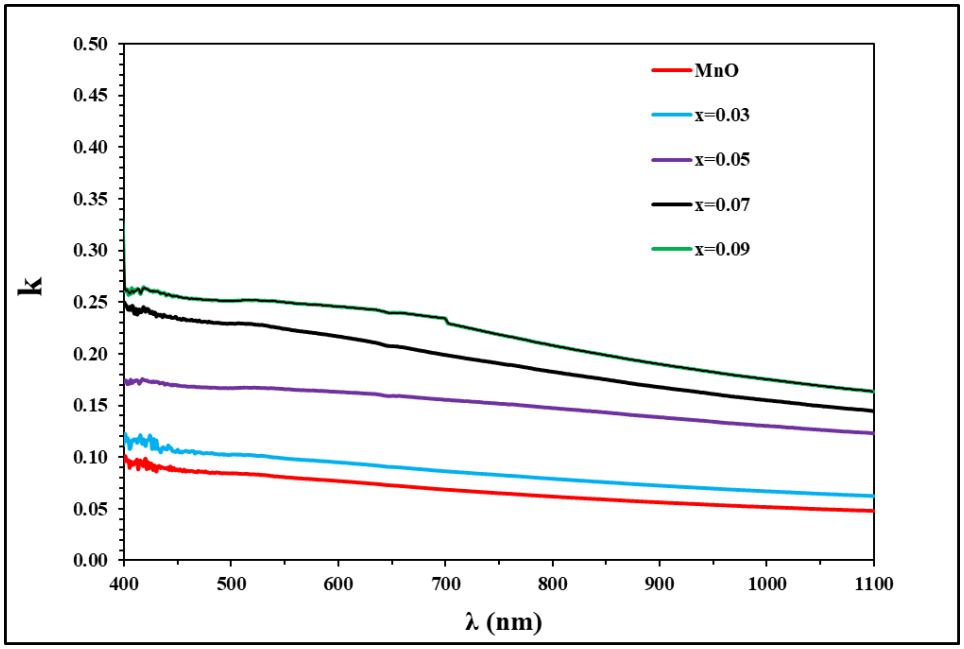

on the absorbance; for this reason, it has the same behavior of increasing with the increase of the Cu content.

Figure 2: Absorbance spectra of the pure and Cu-doped MnO with different Cu content thin films annealed at 473K.

Figure 3: The variation of the extinction coefficient (K) with wavelength for pure and Cu-doped MnO with different Cu concentrations thin films prepared at annealing temperature of 473K.

Fig. 4 shows the variation of the refractive index (n) as a function of wavelength in the range (400-1100) nm for undoped and Cu-doped MnO with different content of Cu annealed at 473 K, which was determined by the following equation [32-37]:

$$n = \frac{1+R}{1-R} + \sqrt{\frac{4R}{(1-R)^2}} - k2 \quad (\mathbf{2})$$

where: R is the reflectance.

It appears from Fig. 4 that the refractive index increased with increasing the Cu content for all prepared samples. It can be noticed from the figure that the refractive index values decreased when annealed at 473k. Mohsin et al. also reported the decrease of the refractive index of annealed samples compared to those for films prepared at RT [38].

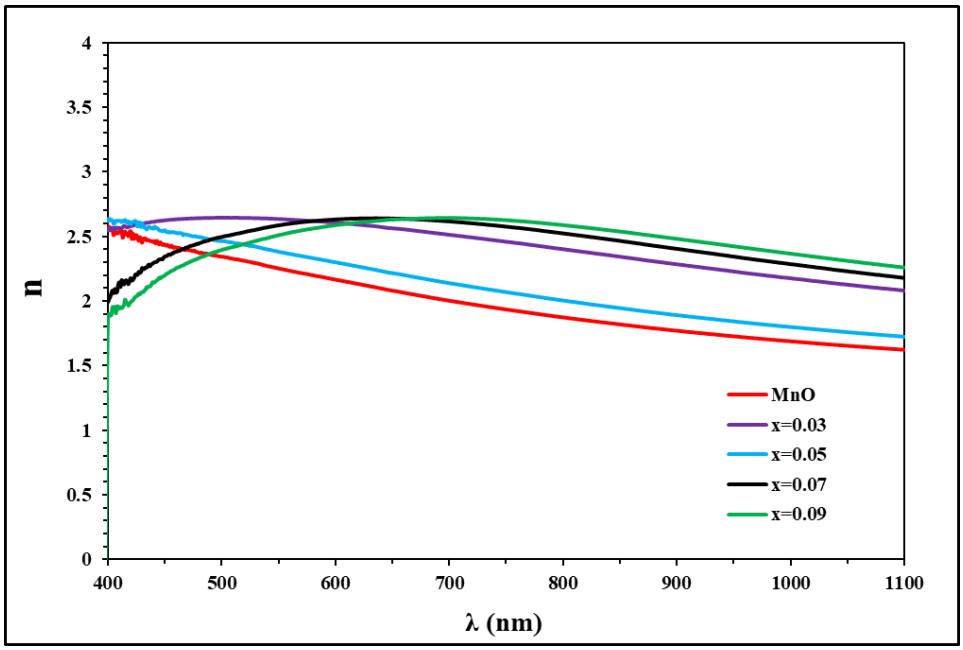

Figure 4: The change in refractive index with wavelength for the pure and Cu-doped with different Cu concentration thin films prepared at annealing temperature of 473k.

Figs. 5 and 6 depict the real (ε_r) and imaginary (ε_i) components of the dielectric constant for the pure and Cu-doped MnO with varying concentrations of Cu (0.03, 0.05, 0.07, and 0.09wt%) thin films annealed at 473 K over the spectral range (400–1100 nm). Using the given equations, the real and imaginary components of the dielectric constant were calculated [39-41]:

$$\varepsilon_r = n^2 - k^2 \quad (\mathbf{3})$$

$$\varepsilon_i = 2nk \quad (\mathbf{4})$$

As shown in Table 2, their values grew as a result of the increase of the dopant concentration.

Table 2: The optical parameters of the thin films of the pure and Cu-doped MnO with different Cu concentrations annealed at 473K.

Sample	K	n	ε_r	ε_i
Pure MnO	0.084	2.344	5.487	0.396
3% Cu :MnO	0.167	2.644	6.963	0.883
5% Cu :MnO	0.102	2.463	6.057	0.503
7 % Cu: MnO	0.230	2.499	6.193	1.148

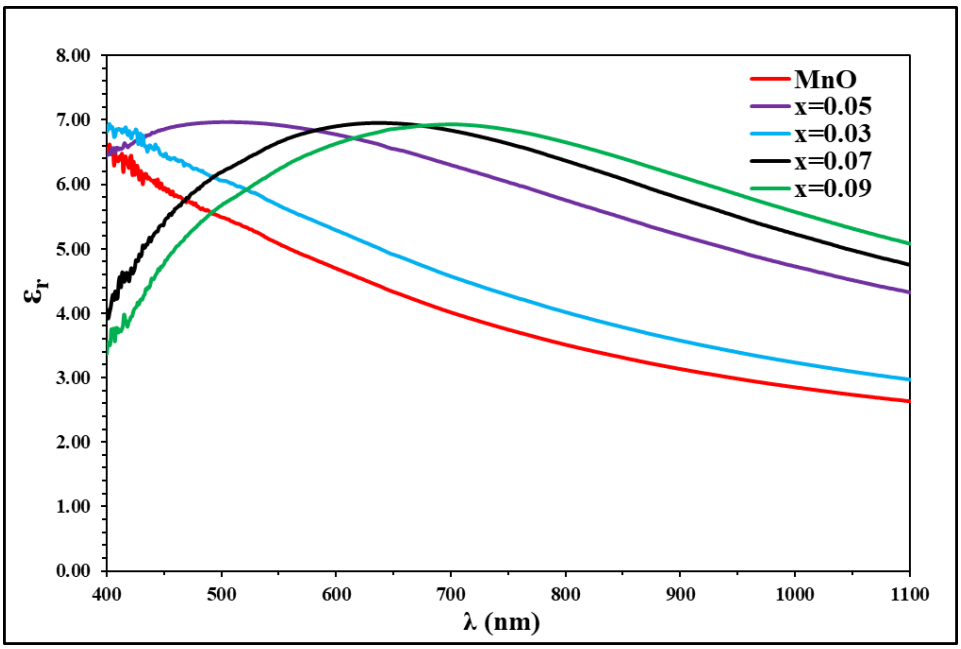

Figure 5: the real part of the dielectric constant for MnO thin films doped with different concentrations of Cu prepared at annealing temperature 473k.

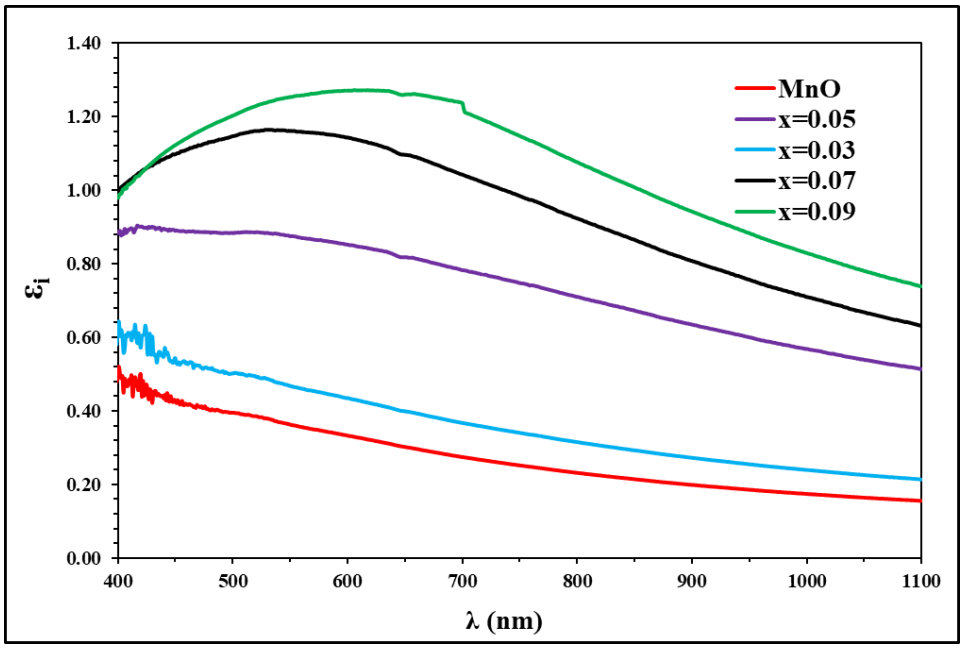

Figure 6: The imaginary part of the dielectric constant for MnO thin films doped with different concentrations of Cu prepared at annealing temperature 473k.

3.3. Hall Effect

Using Hall Effect measurements, thin films of the pure and Cu-doped MnO with varying concentrations of Cu (0.03, 0.05, 0.07, and 0.09 wt%) were examined.
By measuring the Hall voltage (V_H) produced by the Hall field throughout the sample thickness (t), the Hall coefficient (R_H) was calculated [42, 43]:

$$R_H = \frac{V_H}{\mathrm{I}} . \frac{t}{B} \qquad (\mathbf{5})$$

where: I represents the sample current and B represents the magnetic field. Using the given relationship, one can calculate the concentration of carriers [44]:

$$n_H = \frac{1}{e./\ R_H\ /} \quad (6)$$

where: e is the electron charge and (μ_H) is the Hall's mobility measured in (cm^2/V.s) and can be written in the form [45, 46]:

$$\mu_H = \frac{\sigma}{n.e} \quad (7)$$

The Hall coefficient was positive in every sample, indicating p-type conductivity, as shown in Table 3, meaning that the Hall voltage increased as the Cu content increased. with the except of one sample. Also, the results showed that increasing the value of charge carriers (n_H), the mobility (μ_H) and Hall coefficient (R_H) induced an increase in the value of electrical conductivity (σ) with the increase of Cu content. The Hall measurements were performed on samples deposited to ascertain the type and n_H, μ_H, σ and resistivity (ρ) for pure and Cu-doped MnO at annealing temperature (473K).

According to the findings, as Cu concentration rises, an increase was noted in the main parameters resulting in an increase in electrical conductivity (σ). Zahan and Podder [30] have found that the carrier's mobility increased with the annealing temperature(473K) due to the improvement in samples.

Table 3: The Hall mobility, carrier concentration, Hall coefficient, and type of conductivity For the Cu:MnO films doped with varied Cu concentrations and annealed at 473 K.

Sample	σ(1/Ω.cm)	ρ (Ω.cm)	R_H (cm^3/c)	n_H (1/cm^3)	μ(cm^2/V.sec)	type
MnO	5.08E-03	1.968E+03	3.90E+04	1.60E+14	1.98E+02	P
3 % Cu :MnO	4.65E-02	2.151E+01	1.59E+04	3.931E+14	7.38E+02	P
5 % Cu :MnO	1.37E-02	7.299E+01	2.92E+04	2.14E+14	3.99E+02	p
7 % Cu: MnO	1.78E-02	5.617E+01	7.85E+04	4.91E+14	13.972E+02	P
9 % Cu:MnO	5.89E-02	1.697E+03	8.912E+04	5.57E+14	52.49E+02	P

3. Conclusions

This study examines the morphology, optical, and electrical properties of Cu-doped MnO with varying Cu contents; the films were prepared using the PLD process at an annealing temperature of 473K. The morphological results of MnO:Cu films showed that incorporating Cu ions (either +2 or + 1) into the MnO lattice increased the roughness. According to the results of the optical properties study, the film's absorbance decreased but showed high transmittance in the visible range. The absorbance increased as the Cu content rose to 9%. The electrical conductivity, concentration of carriers and Hall mobility increased as the copper content increased. Cu-doped MnO_2 thin films' large crystallite size, regular surface shape, high absorbance, high conductivity, high carrier concentration, and high mobility all point to the material's suitability in optoelectronic devices, gas sensors and biosensors.

Acknowledgments

The authors would like to thank the University of Baghdad, College of Science, Department of Physics for their assistance in carrying out this work.

Conflict of interest

The authors declare that they have no conflict of interest.

References

1. K. A. Aadim Ph D and A. S. Jasim Ph D, Karbala Int. J. Mod. Sci. **8**, 71 (2022).
2. G. Jimenez-Cadena, J. Riu, and F. X. Rius, Analyst **132**, 1083 (2007).
3. G. Korotcenkov, Mater. Sci. Eng. B **139**, 1 (2007).
4. M. A. Abood and B. A. Hasan, Iraqi J. Sci. **64**, 2282 (2023).
5. R. S. Mohammed, K. A. Aadim, and K. A. Ahmed, Karbala Int. J. Mod. Sci. **8**, 88 (2022).
6. A. A. Almaula, Ç. Y. Ataol, and G. H. Mohammed, J. Pharm. Neg. Res. **13**, 936 (2022).
7. Z. N. Majeed, A.-M. E. Al-Samarai, and G. H. Mohammed, Tikrit J. Pure Sci. **23**, 76 (2018).
8. M. Suriyavathana and K. Ramalingam, Int. J. Chem. Tech. Res. **8**, 466 (2015).
9. M. Sharrouf, R. Awad, M. Roumie, and S. Marhaba, Mater. Sci. Appl. **6**, 850 (2015).
10. E. K. Jassem, A. M. A. Majeed, and N. M. Umran, Journal of Physics: Conference Series (IOP Publishing, 2019). p. 012004.
11. S. Ganeshan, P. Ramasundari, A. Elangovan, G. Arivazhagan, and R. Vijayalakshmi, Int. J. Sci. Res. Phys. Appl. Sci. **5**, 5 (2017).
12. S. Thirumalairajan, K. Girija, M. Sudha, P. Maadeswaran, and J. Chandrasekaran, Optoelect. Advan. Mater. Rapid Commun. **2**, 779 (2008).
13. K. J. Kim and Y. R. Park, J. Crys. Grow. **270**, 162 (2004).
14. R. Baca, Mater. Sci. Semicond. Proces. **16**, 1280 (2013).
15. C. Liu, S. Navale, Z. Yang, M. Galluzzi, V. Patil, P. Cao, R. Mane, and F. Stadler, J. All. Comp. **727**, 362 (2017).
16. A. Dakhel, Thin Sol. Fil. **496**, 353 (2006).
17. H. Xia, Y. Wan, F. Yan, and L. Lu, Mater. Chem. Phys. **143**, 720 (2014).
18. F. Chahshouri, E. Khani, H. Savaloni, and R. Savari, SRPH J. Fund. Sci. Tech. **3**, 1 (2021).
19. H. Jamil, M. Khaleeq-Ur-Rahman, I. Dildar, and S. Shaukat, Laser Phys. **27**, 096101 (2017).
20. E. Vlakhov, R. Chakalov, R. Chakalova, K. Nenkov, K. Dörr, A. Handstein, and K.-H. Müller, J. Appl. Phys. **83**, 2152 (1998).
21. K. H. Hwang, S. H. Lee, and S. K. Joo, J. Electrochem. Soci. **141**, 3296 (1994).
22. H. Zhang, G. Cao, Z. Wang, Y. Yang, Z. Shi, and Z. Gu, Nano Lett. **8**, 2664 (2008).
23. O. Erlandsson, J. Lindvall, N. N. Toan, N. V. Hung, V. T. Bich, and N. N. Dinh, Phys. stat. Sol. **139**, 451 (1993).
24. O. Nilsen, H. Fjellvåg, and A. Kjekshus, Thin Sol. Fil. **444**, 44 (2003).
25. L. Feng, Z. Xuan, H. Zhao, Y. Bai, J. Guo, C.-W. Su, and X. Chen, Nanosc. Res. Lett. **9**, 1 (2014).
26. M. Jayandran, M. M. Haneefa, and V. Balasubramanian, J. Appl. Pharmaceut. Sci. **5**, 105 (2015).
27. J. Fei, Y. Cui, X. Yan, W. Qi, Y. Yang, K. Wang, Q. He, and J. Li, Advan. Mater. **20**, 452 (2008).
28. B. P. Kumar, K. Shivaprasad, R. Raveendra, R. H. Krishna, S. Karikkat, and B. Nagabhushana, Int. J. Appl. Innov. Eng. Manag. **3**, 102 (2014).
29. G. Zhang, L. Zheng, M. Zhang, S. Guo, Z.-H. Liu, Z. Yang, and Z. Wang, Ener. Fuels **26**, 618 (2012).

30. M. Zahan and J. Podder, SN Appl. Sci. **2**, 385 (2020).
31. D. T. Mohammed and G. H. Mohammed, E. Euro. J. Phys., 391 (2023).
32. G. H. Mohammed, Iraqi J. Phys. **13**, 82 (2015).
33. K. A. Aadim, N. K. Abbas, and A. T. Dahham, Iraqi J. Sci. **59**, 1567 (2018).
34. A. Hendi, M. Al-Kuhaili, and S. Durrani, Int. J. Res. Eng. Tech. **5**, 320 (2016).
35. M. A. Dahamni, M. Ghamnia, S. E. Naceri, C. Fauquet, D. Tonneau, J.-J. Pireaux, and A. Bouadi, Coatings **11**, 598 (2021).
36. N. A. Daham, A. K. Al-Rawi, and G. H. Mohamed, Ibn Al-Haitham J. Pure Appl. Sci. **23**, 86 (2010).
37. N. Naeema, A. Kudher, and G. H. Mohammed, IOP Conference Series: Materials Science and Engineering (IOP Publishing, 2020). p. 012024.
38. A. N. Mohsin, B. H. Adil, H. Q. Khaleel, R. A. Al-Ansari, and I. R. Swadi, Int. J. Appl. Sci. Tech. **4**, 80 (2022).
39. E. J. Mohammed, A. K. Abbas, and K. A. Aadim, Iraqi J. Phys. **18**, 21 (2020).
40. K. A. Al-Hamdani, Iraqi J. Phys. **8**, 28 (2010).
41. K. A. Adem, Iraqi J. Phys. **5**, 15 (2008).
42. J. Peinke, J. Parisi, O. E. Rössler, and R. Stoop, *Encounter with chaos: self-organized hierarchical complexity in semiconductor experiments* (Germany, Springer Science and Business Media, 2012).
43. H. J. A. Karim and G. H. Mohammed, Iraqi J. Phys. **19**, 75 (2021).
44. C. Iordanescu, D. Tenciu, I. Feraru, A. Kiss, M. Bercu, D. Savastru, R. Notonier, and C. Grigorescu, Dig. J. Nanomater. Biostruct. **6**, 863 (2011).
45. J. Wiley, *Introduction to Solid State Physics* (New York, John Wiley and Sons, 1986), p.185.
46. Z. S. Mahdi and G. H. Mohammed, J. Sur. Fisher. Sci. **10**, 5658 (2023).

تأثير عملية التلدين على الخصائص المورفولوجية والضوئية والكهربائية لأغشية Cu:MnO المحضرة بتقنية ترسيب الليزر النبضي

دعاء ثامر محمد[1] وغصون حميد محمد[1]
[1] قسم الفيزياء، كلية العلوم، جامعة بغداد، بغداد، العراق

الخلاصة

استخدمنا في هذه الدراسة نبضات ليزر Nd:YAG بطول موجي 1064 نانومتر، وقوة 500 مللي جول، وعرض نبضة 9 نانوثانية، وتردد متكرر6 هرتز لتصل إلى السطح المستهدف 300 مرة. تم تحضير عينات غير مطعمه ومطعمه من اغشيه اوكسيد المنغنيز بنسب مختلفه من النحاس (0.03, 0.05, 0.07, and 0.09%) باستخدام طريقه ترسيب الليزر النبضي. تم استخدام تأثير عملية التلدين عند درجة حرارة (473 كلفن) لدراسة الخصائص المورفولوجية والضوئية والكهربائية لأغشية (Cu:MnO). أظهرت نتائج دراسة AFM للخصائص المورفولوجية أن مادة النحاس كان لها تأثير على خلق الخشونة وحجم الجسيمات في أفلام MnO_2. تم فحص النقل البصري باستخدام مقياس الطيف الضوئي UV-Vis. تم اكتشاف أعلى امتصاص بصري عند تركيز 0.09. تمت دراسة المكونات الحقيقية (E_r) والمكونات التخيلية (E_i) لثوابت العزل الكهربائي، بالإضافة إلى معامل الخمود (k)، ومعامل الانكسار (n)، والثوابت الضوئية الأخرى. عند درجة حرارة التلدين (473 كلفن). أظهرت دراسات تأثيرهول أن جميع الأفلام المنتجة تظهر الموصلية نوع P.

الكلمات المفتاحية: الأغشية الرقيقة لاوكسايد المنغنيز، الجسيمات النانوية للنحاس، الثوابت الضوئية ، الخواص المورفولوجية، تقنية ترسيب الليزرالنبضي.